# Transport current carrying superconducting film with periodic pinning array under strong magnetic fields

B. Rosenstein,[1,2] I. Shapiro,[3] and B. Ya. Shapiro[3]

[1]*Department of Electrophysics, National Chiao Tung University, and the National Center for Theoretical Sciences, Hsinchu, Taiwan, Republic of China*

[2]*Applied Physics Department, Ariel University Center of Samaria, Ariel 40700, Israel*

[3]*Department of Physics, Institute of Superconductivity, Bar-Ilan University, 52900 Ramat-Gan, Israel*

(Received 8 September 2010; revised manuscript received 7 November 2010; published 22 February 2011)

The transport current carrying dissipative (flux flow) and dissipationless (pinned) vortex configurations and their dynamics are investigated numerically in the framework of the time-dependent Ginzburg-Landau approach. Assuming that magnetic induction is nearly uniform, the model is generalized to include strong inhomogeneous electric fields. Hexagonal array nanoholes of the size of coherence length and density $n_{\rm pin}$ was considered for various filling factors [defined as $f = B/(\Phi_0 n_{\rm pin})$]. The vortex depinning is closely associated with the appearance of a strongly varying electric field. For the matching field, $f = 1$, the critical current is maximal and the transition to the resistive state occurs as a coherent depinning of the entire vortex lattice. For a system with interstitial vortices, $f > 1$, the mechanism of depinning depends on the current direction with respect to the pinning array. There are two qualitatively distinct geometries: the obstacle and channel geometries. In the obstacle geometry lines of interstitial vortices are blocked by strongly pinned vortices, while in the channel geometry the lines move unimpeded confined in channels. It was found that slightly above the critical current the trajectories of the moving vortices are not straight, but rather acquire a snakelike shape enveloping the system of pins. In contrast to $f = 1$, the transition to a resistive state is not coherent and is going through formation of "snakelike" vortex trajectories. The critical current in the obstacle geometry is significantly larger than in the channel one.

DOI: 10.1103/PhysRevB.83.064512 PACS number(s): 74.20.De, 74.25.Wx, 74.25.Sv

## I. INTRODUCTION

The great interest in the problem of magnetic-flux pinning in type-II superconductors is associated with its relevance to technological applications of superconductivity. However, in magnetic fields the zero resistance property of the superconductors is lost owing to the dissipative motion of the magnetic flux (Abrikosov vortices) in a form of flux flow or creep. In order to restore the superconductivity one has to find an efficient way to block the flux flow by "pinning" of the vortices. An important challenge in applications of type-II superconductors is achieving optimal critical currents $J_c(B)$ under an applied magnetic field $B$. Below this current the vortex matter is under sustainable stress (vortices being displaced) and can support a dissipationless electric current. The critical current decreases as magnetic induction increases and consequently the pinning efficiency should be optimized. Although intrinsic pinning always exists in bulk superconductors, it is rather inefficient at elevated fields. Recently a new possibility has been developed—pinning by artificially assembled well-controlled periodic arrays of holes[1] and magnetic dots[2] (for a review, see Ref. 3).

It was predicted theoretically in the framework of the London model[4–6] and confirmed[1,2,7,8] experimentally at low magnetic fields that, when pinning centers are arranged into a periodic array commensurate with the Abrikosov lattice, the critical current increases dramatically. Technological progress leads to smaller sizes of the pinning centers often comparable with the coherence length $\xi$ of a superconductor, while the range of the magnetic fields continuously increases. Alternatively the coherence length can be significantly increased by tuning temperature to be just below critical $T_c$. The critical current is maximized when the nanohole's lattice is hexagonal at the matching field $B = \Phi_0 n_{\rm pin}$, where $\Phi_0$ is a unit of flux and $n_{\rm pin}$ is the density of pins. This case was treated analytically in the framework of the Ginzburg- Landau (GL) theory.[9]

When the number of vortices exceeds that of the pinning centers, namely, when the filling factor $f = B/(\Phi_0 n_{\rm pin}) > 1$, additional, "interstitial" vortices appear. Although not directly pinned by the pinning centers, they strongly interact with the pinned vortex subsystem (PVS) and with each other. As a result the flux in this case can be clearly separated into two subsystems: a mobile, weakly pinned interstitial vortex subsystem (IVS) and almost rigidly pinned PVS. Obviously the interstitial vortices reduce the critical current, because they are pinned just by a repulsive potential created by the static PVS. It is one of the purposes of the present paper to point out that IVS possesses universal static and dynamic properties in a sense that they do not depend on the microscopic details of the pinning potential (because an interstitial vortex interacts only with a rigidly pinned vortices). For $f > 1$ it turns out that the critical current is very anisotropic with respect to orientation of the current relative to that of the primitive vector of the unit cell of the pinning array.

Theoretically two models are used to describe the vortex system with a periodic array of pinning centers under stress of the transport current. In the first model the vortices are treated (numerically) as interacting two-dimensional (2D) points subjected to a periodic pinning potential and the driving force.[4–6] The (pairwise) interaction potential is taken to be that following from the London approximation. This approach is appropriate to describe weak magnetic fields and sparse pinning arrays, so that the structure of the vortex

 

core can effectively be ignored. Within the London model [supposed to be applicable as low magnetic inductions far from the upper critical field $H_{c2}(T)$] vortices interact within the range of order of magnetic penetration depth $\lambda$. A very comprehensive numerical work on the vortex "gas"[4–6] revealed static configurations of the interstitial vortices for various rational $f$ 's and the nature of the flux flow. A profound asymmetry with respect to the direction of motion was found for $f > 1$. In addition, it turned out, as expected,[5] that the motion occurs in channels, however, the vortex trajectories may be either straight or follow a bottom valley of the potential landscape in a zigzag-shaped form. The *I-V* curves were numerically determined (even in the presence of thermal fluctuations) and the critical current calculated.

A question arises as to whether these general features persist in strong magnetic fields or when the pinning centers are small and distances become not very large compared to coherence length (in many recent experiments $\lambda$ is much larger than distances between nanoholes). As mentioned above, in this qualitatively distinct situation, when the interaction between the vortices is long range and collective, one has to consider the GL model. Recently, however, the arrays are fabricated on the nanoscale and the range of fields applied continuously increases. Therefore the distribution of the order parameter becomes of importance and one has to resort to a complementary approach. Because microscopic theory in the inhomogeneous situation is not practical, the only available tool at large fields and nanosize pinning arrays is the GL phenomenological approach.[10,11] The approach simplifies considerably when magnetic induction exceeds significantly the lower critical field $H_{c1}(T)$. The distribution of the magnetic induction becomes practically uniform and the only dynamic degrees of freedom are the order parameter $\Psi$ and electric field $E$.

A modern application of the time-dependent GL (TDGL) approach to the vortex dynamics in large 2D samples should include four ingredients: (a) a (strong) magnetic field creating a strongly correlated vortex system; (b) a periodic pinning array; (c) a bias current that governs vortex motion (but does not create additional vortices) and transport current; and (d) effects of the electric field especially important in the depinning process. The problem, incorporating (b), (c), and (d), was first formulated in Ref. 12. In a recent comprehensive study,[13] (a), (c), and (d) are present (the transport current, however, creates vortices and antivortices near the boundary). In a series of works,[14] static configurations and stability with respect to current were comprehensively explored (which allows determination of the critical current), but purely dynamics effects such as electric field (and the corresponding normal current) are not considered. The vortex dynamics under an ac field was considered analytically in a linear response approximation for integer $f$ in Ref. 15, and an exact expression for the ac case was obtained. However, a general approach to dynamics requires an essential modification, because a linear response fails and effects of the inhomogeneous electric field produced by the vortex motion have to be accounted.

In the present paper we consider both the static (stationary) and the dynamic properties of the vortex matter in commensurate pinning arrays for several filling factors $f \geqslant 1$. The asymmetry is investigated by considering two extreme cases.

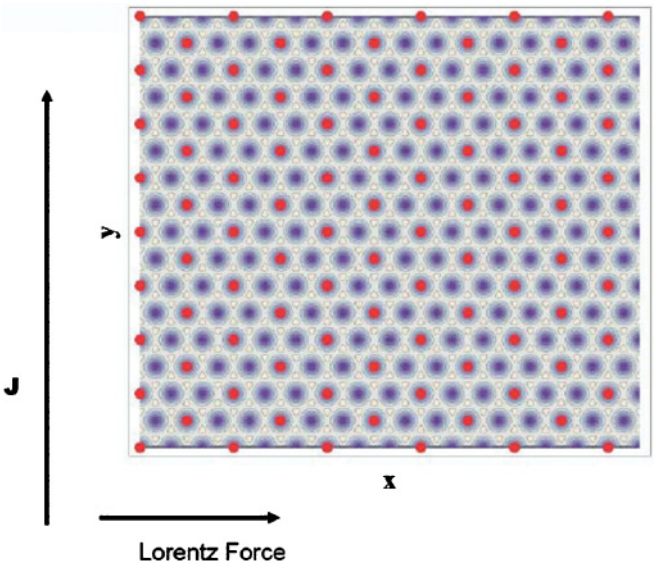


FIG. 1. (Color) Obstacle geometry for $f = 3$. Distribution of the superfluid density $|\psi(\mathbf{r})|^2$ of the hexagonal static Abrikosov vortex lattice (not carrying the transport current) is shown. The electric field and the transport current will be directed along the $y$ axis, and would create a Lorentz force at the $x$ direction. A third of the zeros of the order parameter in the equilibrium state fall on the locations of the pins (red blobs). In this case the direction of the flux motion might be blocked by the pinning sites.

One is an "obstacle" (see, for example, Fig. 1 for $f = 3$), when a row of pinning centers blocks a line of interstitial vortices, while another is a "channel" (see Fig. 2 for $f = 4$), when the interstitial vortices can move unimpeded. Sometimes the difference between the two is that the current is rotated with respect to a basis vector of the pinning array. In particular, for $f = 3$, the channel geometry is obtained from that of the Fig. 1 by rotation of the transport current by 30°.

The paper is organized as follows. A general GL setup including effects of the electric field in dynamics are described in Sec. II. Discretization and a numerical method

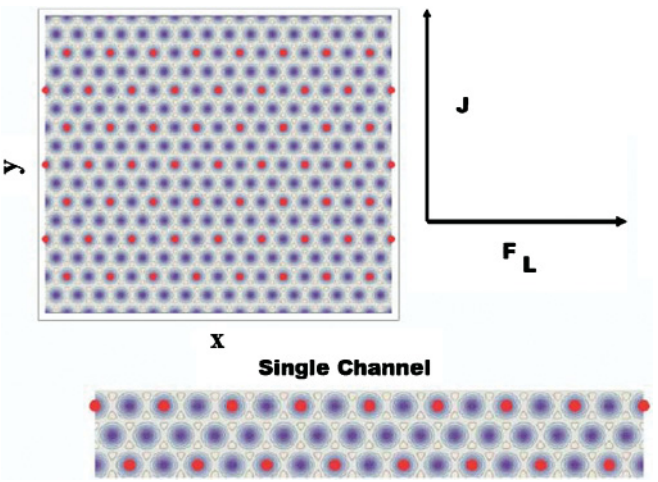


FIG. 2. (Color) Channel geometry for $f = 4$. Motion of the interstitial vortices in chains between the pinning raws is unimpeded.

are also briefly described. Results for the stationary current carrying states and dynamics are described in Sec. III. A summary and a discussion are the subjects of the concluding Sec. IV.

## II. ELECTRODYNAMICS OF TYPE-II SUPERCONDUCTORS IN STRONG MAGNETIC FIELD

### A. Basic equations

We consider a superconducting slab subjected to a sufficiently high, homogeneous, and time-independent magnetic induction perpendicular to the slab $\mathbf{B} = B\hat{\mathbf{z}}$. Assuming that the ratio $\kappa \equiv \lambda/\xi \gg 1$, the magnetization is smaller than the field by the factor $1/\kappa^2$; consequently, for magnetic fields several times larger than $H_{c1}$, $B \approx H$ and is practically homogeneous and is therefore treated as a constant rather than a degree of freedom. In thin films this condition is satisfied because the penetration depth becomes $\lambda_{\rm eff} = 2\lambda^2/d$, where the thickness provided by the film width $w$ is small enough ($w < \lambda_{\rm eff}$). In what follows we consider an effective 2D model.

The time-dependent GL equation for a dimensionless order parameter $\psi$ and scalar potential $\phi$ has the form

$$\frac{\partial\psi}{\partial\tau} + i\phi\psi = -\frac{\delta}{\delta\psi^*} f_{\rm GL}[\psi], \tag{1}$$

where

$$f_{\rm GL} = \int d^2\mathbf{r}\left\{\psi^*\left[-\frac{D^2}{2} - \frac{1-t}{2} + V_{\rm pin}(\mathbf{r})\right]\psi + \frac{1}{2}(\psi^*\psi)^2\right\} \tag{2}$$

is the GL free energy. The covariant derivatives $\mathbf{D} \equiv \nabla - i\mathbf{A}$ include the vector potential $\mathbf{A} = b(-\frac{1}{2}y, \frac{1}{2}x, 0)$, describing the magnetic induction [$b = B/H_{c2}(T)$]. In our gauge the electric field is $E = -\nabla\phi$. Equation (1) is supplemented by the charge conservation law,

$$\nabla \cdot \mathbf{j} = 0, \tag{3}$$

where the dimensionless current density, including the normal component, is given in our gauge by

$$\mathbf{j} = \frac{i}{2}[\psi^*\mathbf{D}\psi - \psi(\mathbf{D}\psi)^*] - \nabla\phi. \tag{4}$$

The coherence length $\xi$ will be used as a unit of length $\mathbf{r} \to \mathbf{r}/\xi$. The dimensionless order parameter $\psi$ is scaled by the square root of the superfluid density.[9,15,16] The reduced temperature is $t = T/T_c$, while the current density is written in the units of the depairing current,

$$J_d = \frac{cH_{c2}}{2\pi\xi\kappa^2}. \tag{5}$$

In analogy to the coherence length, one can define a characteristic time scale. In the superconducting phase this is a typical "relaxation" time:

$$\tau = t/t_{\rm GL}, \quad t_{\rm GL} = \gamma\xi^2/2, \tag{6}$$

where $\gamma$ is the inverse electron diffusion constant, and the unit of electric field is

$$E_{\rm GL} = H_{c2}\frac{\xi}{ct_{\rm GL}}. \tag{7}$$

The conductivity will be given in units of

$$\sigma_{\rm GL} = \frac{c^2 t_{\rm GL}}{2\pi\lambda^2} = \frac{c^2\gamma}{4\pi\kappa^2}. \tag{8}$$

This unit is close to the normal state conductivity in low $T_c$ superconducting metals in the dirty limit $\sigma_n = \frac{c^2\gamma}{8\pi\kappa^2}$.[11] More generally, there is a factor $k$ of order 1, $\sigma_n = k\sigma_{\rm GL}$.

The potential $V_{\rm pin}$ describes a $\delta T_c$ pinning array [17] $V_{\rm pin}(\mathbf{r}) = \sum_a V(\mathbf{r} - \mathbf{r}_a)$, where $\mathbf{r}_a$ denote the locations of the nanoholes centers. A simplest model of a hole (or a dielectric inclusion) is that one forces the order parameter to vanish at these locations. In a geometry considered here (see Figs. 1 and 2), the applied dc current will be always oriented along the $y$ axis. Different relative orientations with respect to the pinning array will be studied by rotating the pinning array. This is more convenient for simulations owing to the need to impose boundary conditions. The system of equations should be complemented by the following boundary conditions:

$$-\nabla_y\phi = j^{\rm ext}|_{y=0,L_y}, \quad \nabla_x\phi = 0|_{y=0,L_y}, \tag{9}$$

where $L_y$ is the length of the sample in the current direction $y$. Periodic boundary conditions in the perpendicular $x$ direction are assumed. The order parameter is therefore subject to "metallic electrode" boundary conditions,

$$\psi = 0|_{y=0,L_y}, \tag{10}$$

and periodic under magnetic translations (see the following for a detailed definition) in the $x$ direction.

### B. Discretized form of the electrodynamics of the strongly type-II superconductors

The above equations were treated numerically using Wilson's discretization.[18] The points on the grid (in units of $\xi$),

$$\mathbf{r}_{\mathbf{n}} = (n_1 a_x, n_2 a_y), \tag{11}$$

are labeled by two integers, $n_1 = 1, \ldots, n_{\rm max}$ and $n_2 = 0, \ldots, n_{\rm max}$. The grid lattice spacings are $a_x^2 = \frac{4\pi}{\sqrt{3}bs}$ and $a_y^2 = \frac{\sqrt{3}\pi}{bs}$, where $s$ is an integer. Our sample has the aspect ratio of $\frac{L_y}{L_x} = \frac{\sqrt{3}}{2}$ with $n_{\rm max} = sN^{1/2}$, so that number of vortices is $N$.

The constant homogeneous magnetic field is described by the Wilson link phases,[18] $\theta^{\gamma}_{n_1,n_2}$,

$$U^{\gamma}_{n_1,n_2} = \exp\left(i\theta^{\gamma}_{n_1,n_2}\right), \tag{12}$$

$$\theta^1_{n_1,n_2} = -\frac{\pi}{s^2}n_2, \quad \theta^2_{n_1,n_2} = \frac{\pi}{s^2}n_1. \tag{13}$$

Periodic (magnetic) boundary conditions for the rectangular sample read[17]

$$\psi_{0,n_2} = \exp\left(i\frac{\pi n_{\rm max}}{s^2}n_2\right)\psi_{n_{\rm max},n_2}, \tag{14}$$

$$\psi_{n_{\rm max}+1,n_2} = \exp\left(-i\frac{\pi n_{\rm max}}{s^2}n_2\right)\psi_{1,n_2},$$

$$\psi_{n_1,0} = 0, \quad \psi_{n_1,n_{\rm max}} = 0. \tag{15}$$

The corresponding boundary conditions for the scalar potential are

$$\begin{gathered}\phi_{0,n_2}=\phi_{n_{\max},n_2},\quad \phi_{n_1,0}=\phi_{n_1,n_{\max}},\\ \phi_{n_1+1,0}-\phi_{n_1,0}=0,\quad \phi_{n_1+1,n_{\max}}-\phi_{n_1,n_{\max}0}=0,\\ \phi(0,0,0)=0,\\ \frac{1}{a_y}\left(\phi_{n_1,1}-\phi_{n_1,0}\right)=-j^{\text{ext}},\\ \frac{1}{a_y}\left(\phi_{n_1,n_{\max}}-\phi_{n_1,n_{\max}-1}\right)=-j^{\text{ext}},\\ \frac{1}{a_x}\left(\phi_{n_1+1,0}-\phi_{n_1,0}\right)=0,\quad \frac{1}{a_x}\left(\phi_{n_1+1,n_{\max}}-\phi_{n_1,n_{\max}}\right)=0.\end{gathered}\tag{16}$$

The discretized TDGL equations are

$$\left(\frac{d}{d\tau}-i\phi_{n_1n_2}\right)\psi_{n_1,n_2}=\frac{s^2b\sqrt{3}}{8\pi}\left[\begin{array}{c}U^1_{n_1,n_2}\psi_{n_1+1,n_2}+\frac{4}{3}U^2_{n_1,n_2}\psi_{n_1,n_2+1}\\ +U^{1*}_{n_1-1,n_2}\psi_{n_1-1,n_2}+\frac{4}{3}U^{2*}_{n_1,n_2-1}\psi_{n_1,n_2-1}-\frac{14}{3}\psi_{n_1,n_2}\end{array}\right]+\frac{1-t}{2}\psi_{n_1,n_2}-|\psi_{n_1,n_2}|^2\psi_{n_1,n_2}.\tag{17}$$

In addition, they are supplemented by the Poisson equation

$$\nabla^2\phi=i\frac{s^2b\sqrt{3}}{8\pi}\psi^*_{n_1,n_2}\left[\begin{array}{c}U^1_{n_1,n_2}\psi_{n_1+1,n_2}+\frac{4}{3}U^2_{n_1,n_2}\psi_{n_1,n_2+1}\\ +U^{1*}_{n_1-1,n_2}\psi_{n_1-1,n_2}+\frac{4}{3}U^{2*}_{n_1,n_2-1}\psi_{n_1,n_2-1}-\frac{14}{3}\psi_{n_1,n_2}\end{array}\right]+\text{c.c.}\tag{18}$$

Strong pinning is introduced by "excluding" a point from the grid. This means that the order parameter vanishes at these points. The supercurrent density is discretized as

$$\begin{aligned}j^{s1}_{n_1,n_2}&=\frac{i}{2a_x}\psi^*_{n_1,n_2}U^1_{n_1,n_2}\psi_{n_1+1,n_2}+\text{c.c.},\\ j^{s2}_{n_1,n_2}&=\frac{i}{2a_y}\psi^*_{n_1,n_2}U^2_{n_1,n_2}\psi_{n_1,n_2+1}+\text{c.c.}\end{aligned}\tag{19}$$

The numerical method utilized is the Crang-Nickolson algorithm. The initial condition was set by the Abrikosov analytic expression.[17] Evolution in time settled after several thousands of time steps of order $\Delta\tau=0.001t_{\text{GL}}$. The magnetic field is taken as $b=0.5$ and the temperature $t=0$ was constant throughout our simulations. Variation of these parameters does not change qualitatively the results of our study. No thermal fluctuations on the mesoscopic scale were introduced, although an insignificant grid noise was present. The pinned area of one pinning center corresponds to one point of the grid, simulating radius of the pinning center of approximately $a/s$. We always used $s=16$ corresponding to $16\times16$ grid points per vortex. The number of vortices was always quite large, $16\times16=256$, to overcome boundary effects. In the middle of our sample (in the current direction,$y$) the dynamics is independent of the edge effects owing to the metallic leads. These effects are interesting in their own right and clearly seen on all our figures. Unlike the analytic method, the simulation can be performed for arbitrary filling fractions.

Now we proceed to a description of the results for various filling factors and transport currents.

## III. CURRENT CARRYING VORTEX STATES

Vortex matter in the presence of pinning and carrying transport electric current has one static and two dynamic phases. Electric current acts as a driving force on the vortex matter, and there is an intricate interplay between the stress and the elasticity of the vortex matter and the pinning strength. The phase boundary between the static phase and a moving (flux flow or creep) phase is determined by the critical current as function of parameters of the system: magnetic field, temperature, and pinning strength. First we consider the structure of the static, albeit current carrying, vortex state in the presence of various hexagonal pinning structures with an integer filling factor $f\geqslant1$. It turns out that the elastic properties of the vortex matter are markedly different for the matching field, $f=1$, and when interstitial vortices are present, $f>1$. In both cases dynamics and the voltage-current ($I$-$V$) characteristics are investigated.

Within the GL approach, although the magnetic field is practically uniform and "magnetic fluxons" do exist, one has well-defined vortex-type distributions of the complex order parameter $\psi(\mathbf{r})$. Below we call the area in which the superfluid density, $|\psi(\mathbf{r})|^2$, is significantly suppressed as a "vortex" core. In the studied field range the vortices are extended objects having a shape, not just "points." Under the stress created by the transport current vortices are deformed and shifted from their equilibrium position (defined when the transport current is absent).[9] Below the critical current vortices are displaced in the direction perpendicular to that of the persistent current, while the electric field vanishes. The critical current is determined by the stability of the static distorted Abrikosov lattice carrying a net supercurrent. Above the critical current the electric field becomes nonzero and vortices start to move. We focus on the mechanism of depinning, especially on the emerging strong and inhomogeneous electric fields just above the critical current.

### A. Matching field, $f=1$

In this simplest situation there is one vortex per pinning site. We assume here that the pinning array is hexagonal and therefore does not conflict with the preferred lattice structure of the vortex matter. It was assumed in a recent analytic calculation[9] that, although the distribution of the order parameter under current evidently loses rotational hexagonal symmetry (technically owing to an admixture of higher Landau levels, see Ref. 9), the unit cell still contains a single vortex. As Fig. 3(a) demonstrates, this is indeed the case. Indeed, the

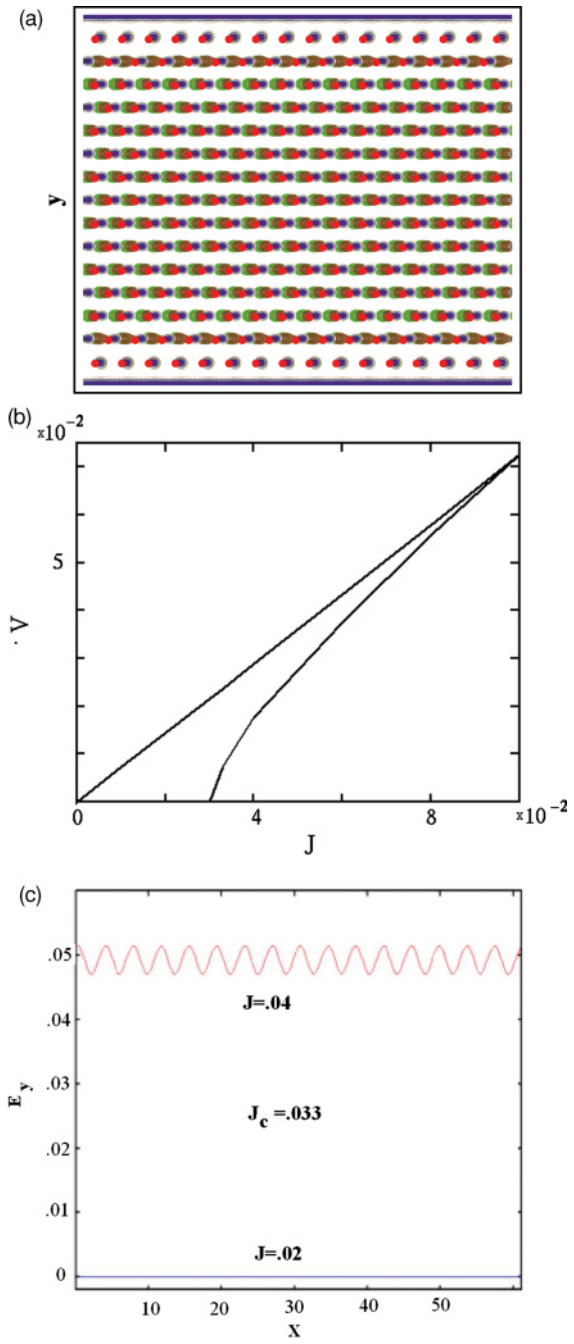


FIG. 3. (Color) Structure, the *I-V* curve, and electric field at matching field. There is one vortex per pinning site (red blob), so that the filling factor $f = 1$. Magnetic field $B = 0.5H_{c2}$ and temperature is zero. (a) Coherent motion of the vortex lattice. Distribution of the superfluid density $|\psi(\mathbf{r})|^2$ at three consequent times (depicted by blue, green, and brown couture plots) given. The value of the current is $j = 0.04$, larger than the critical value of $j_c = 0.033$ . The structure of the coherently moving lattice supports the analytical result of Ref. 9. (b) The dc *I-V* curve for matching field. The Bardeen-Stephen law is shown by a straight line for comparison. The critical current is very high, $j_c = 0.033$ in units of the depairing current, Eq. (5). (c) Local electric field distribution. Profile of electric field [in units of $E_{\mathrm{GL}}$, see Eq. (7)] for $y = L_y/2$ as function of $x$. Below $j_c$ at $j = 0.02$ electric field is zero, while above $j_c$ at $j = 0.04$ electric field is constant on average, but shows small sinusoidal deviations owing to the vortex lattice structure.

vortices move coherently when the current exceeds ($j = 0.04$) the critical one.

The critical value $j_c = 0.033$ [in units of $J_d$ defined in Eq. (5)] determined from the *I-V* curve [Fig. 3(b)] is in a good agreement with the result obtained analytically in the framework of the variation procedure (see Fig. 3 of Ref. 9 for the deltalike potential with strength of order one). The electric field plays a major role in the process of depinning. While below the critical current at $j = 0.02$, it is strictly zero everywhere [see the lower line in Fig. 3(c)] (the value of a random field is consistent with zero at our level of noise), above it [at $j = 0.04$, upper line in Fig. 3(c)] the electric field is constant on average, but shows small sinusoidal deviations owing to the vortex lattice structure. Numerical simulations demonstrate that the resistive state occurs by a coherent depinning, as it was assumed in the analytic work[9] [see Fig. 3(a)]. The mechanism of depinning consists of a series of sudden jumps from one pinning center to its neighbor along the vortex trajectory line with replacement of the vortex on this site.

The situation is different when interstitial vortices are present for $f > 1$.

### B. Interstitial vortices in obstacle pinning array for $f = 3$

In the equilibrium (currentless) state the interstitial vortices in this case are locked by the strongly pinned vortices that are located on the pinning centers (PVS) (see Fig. 1). Vortex matter as a whole remains static up to a sufficiently large magnitude of the transport current, $j_c = 0.0073$. Above this value, for example, at $j = 0.0075$, the interstitial vortices show a sinusoidal-like instability ("snakes") forming the structure enveloping the PVS [Fig. 4(a)]. These snakes move, destroying the static vortex phase and creating voltage. The number of the vortex snakes increases along with the transport current, until the interstitial vortices start to push out the strongly pinned vortices and replace them. In the moving vortex matter at $j = 0.01$, all of the vortices participate in laminar stream [Fig. 4(b)]. The voltage current characteristics (Fig. 5) show a strong decrease of the critical current in comparison to the case of the matching field. The situation is qualitatively different, when channels are available. In this case the critical current is further reduced. This happens, for example, when the current direction does not coincide with the principle axis of the pinning lattice. We exemplify this generic situation on the simplest case of $f = 4$.

### C. Interstitial vortices in channel pinning array for $f = 4$

The mechanism of destruction of the superconductivity by creation of a resistive state by the current is essentially different in this case than that in the obstacle pinning array geometry. At least some of the interstitial vortices in this case are confined inside the channels formed by the line of alternating strongly pinned and interstitial vortices (see Fig. 2). The interstitial vortices in the channel are very slightly pinned. However, even in this case, the interplay between vortex matter elasticity, the interaction with the vortices forming the channel walls, and the transport dc current result in the existence of various dynamic vortex phases. As current increases, the system undergoes a

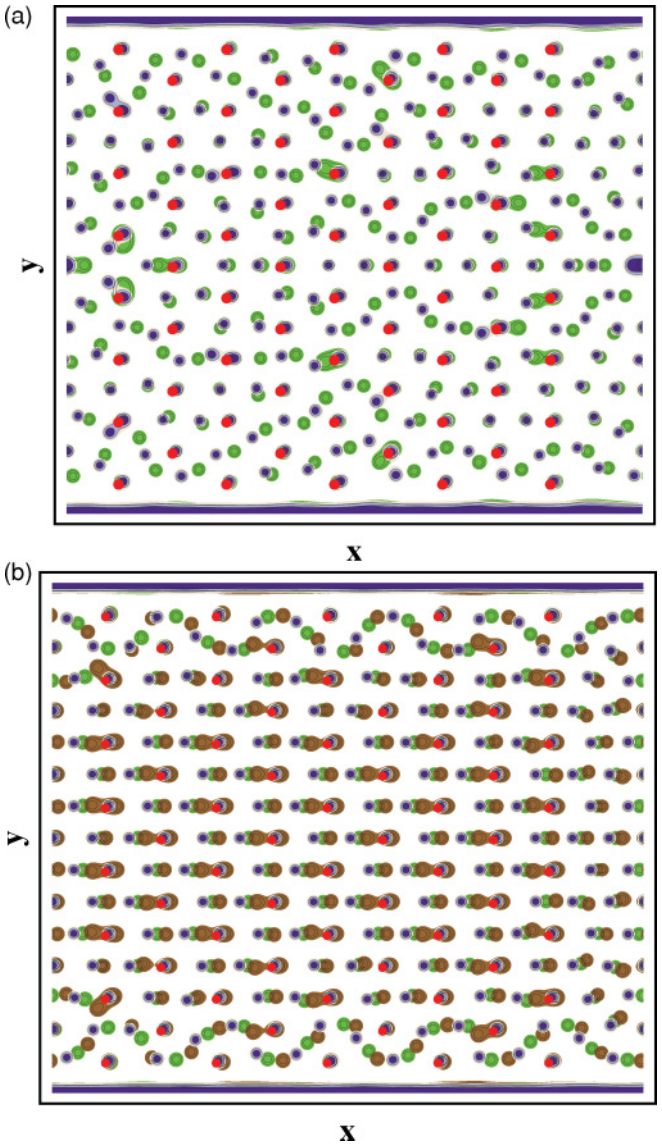


FIG. 4. (Color) Structure of the pinned and the flux flow states for the obstacle geometry for $f = 3$. Snapshots of the distribution of the superfluid density at three consecutive times are shown as green, red, and brown contours. (a) Just above the critical current $j_c = 0.0073$ at $j = 0.0075$. One observes that there are snakelike interstitial vortex trajectories around PVS. (b) Above the critical current, $j = 0.01$. One observes that there are streamlike straight trajectories of all of the vortices. The vortices of the PVS are pushed out from the pinning sites and replaced by the interstitial vortices.

transition from the static pinned state to the moving incoherent (snake) phase, followed by the coherent motion.

In more detail, just above the critical current $j_c = 0.003$ at $j = 0.004$, the snakelike vortex phase inside the channels appears [see Fig. 6(a)]. The transition to a resistive state is owing to the snakelike instabilities, although interstitial vortices trapped inside the channel walls are eventually also involved. At large currents all of the vortices are completely depinned. In this case both the vortices of the former channels and those that formed PVS participate in coherent laminar stream motion [see Fig. 6(b)]. The voltage-current

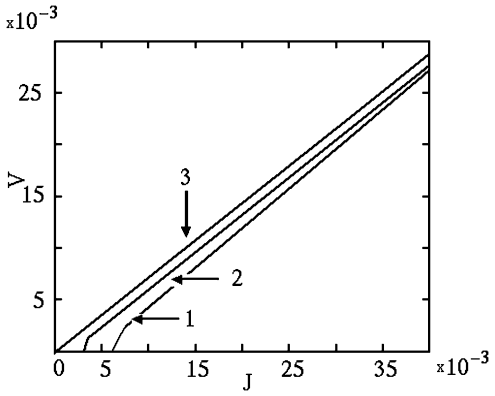


FIG. 5. The $I$-$V$ characteristics of the pinning array with interstitial vortices. Curve 1 is the voltage-current characteristics for the obstacle geometry for $f = 3$, while curve 2 is the $I$-$V$ for the channel geometry for $f = 4$. It demonstrates a small critical current in comparison with the obstacle geometry. Line 3 is the Bardeen-Stephen law.

characteristic in this case demonstrates extremely small critical currents (Fig. 5).

The vortex depinning is accompanied by the appearance of slightly varying electric field (on the scale of the coherence length) already at the current $j = 0.002$, just below $j_c = 0.003$ (see the lower three lines for three consequent times in Fig. 7). The electric field becomes strongly oscillating (the upper three lines in Fig. 7) for $j = 0.004$ just above $j_c$.

## IV. SUMMARY AND DISCUSSION

To summarize, we investigated the structure and dynamics of the current carrying state in type-II superconductors with periodic array of nanoholes under strong magnetic fields. The transport current carrying dissipative (flux flow) and dissipationless (pinned) configurations were investigated numerically in the framework of the time-dependent GL approach generalized to include strong inhomogeneous electric fields (that are necessarily created when the vortex system depins). We have limited ourselves to the case of hexagonal pinning arrays with filling factors $f = 1,3,4$ with currents ranging from a fraction of the depinning current to several critical currents. Strong pinning (a hole or a dielectric inclusion) of the size of order of coherence length was assumed.

A maximal critical current of 4% of the depairing current $j_d$ is obtained for the matching field $f = 1$. The mechanism of depinning consists of a series of sudden jumps from one pinning center to its neighbor along the vortex trajectory line, with replacement of the vortex on this site. The situation is different when interstitial vortices are present, $f > 1$. The system with interstitial vortices ($f > 1$) is highly anisotropic with respect to the current direction with respect to the unit cell of the pinning array. The critical current depends strongly on the orientation, and a maximal value of $6.5 \times 10^{-3}$ is achieved for the obstacle geometry. For an example of $f = 3$, such an arrangement of the pinning array and the current direction is shown in Fig. 1. It was found that slightly above the critical current the trajectories of the moving vortices are not straight but rather acquire a snakelike shape enveloping the system of pins.

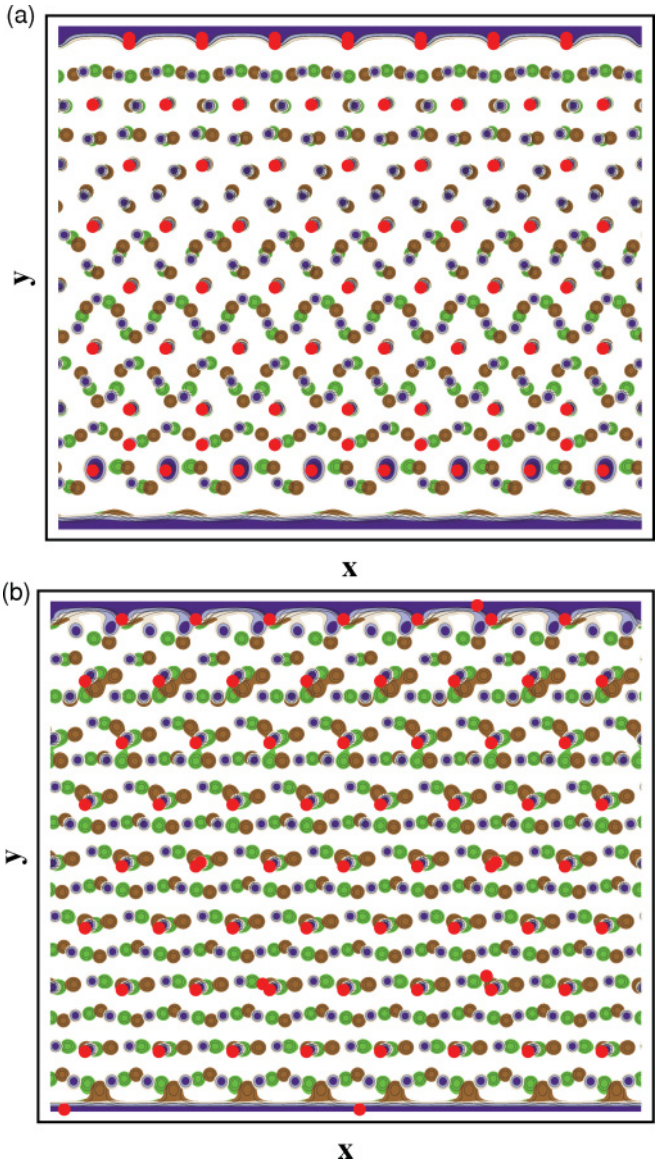


FIG. 6. (Color) Structure of the pinned and the flux flow states for the channels geometry for $f = 4$. (a) Just above the critical current $j_c = 0.003$ at $j = 0.004$. Interstitial vortices in the channels become unstable, forming a snakelike vortex structure. (b) Above the critical current, $j = 0.04$. Both interstitial vortices and PVS flows. One observes that there are streamlike straight trajectories.

In contrast to $f = 1$, in this case the transition to a resistive case does not occur by a substitution of the strongly pinned vortices, but the vortex matter separates into two subsystems: static pinned vortices, PVSs, and moving "snakes," IVSs. In the channel geometry (see Fig. 2), the critical current is further reduced. For example, in the case of $f = 4$ we obtain $1.5 \times 10^{-3}$. In this case the transition to the resistive state takes is accompanied by formation of snakes inside the channels. At larger currents the structure of the current carrying state is universal. The vortices are ripped off and move coherently along straight trajectories.

The transition to a resistive state is accompanied by the appearance of rather strong electric fields, shown in Figs. 3(c) and 7. The electric field becomes homogeneous in accordance

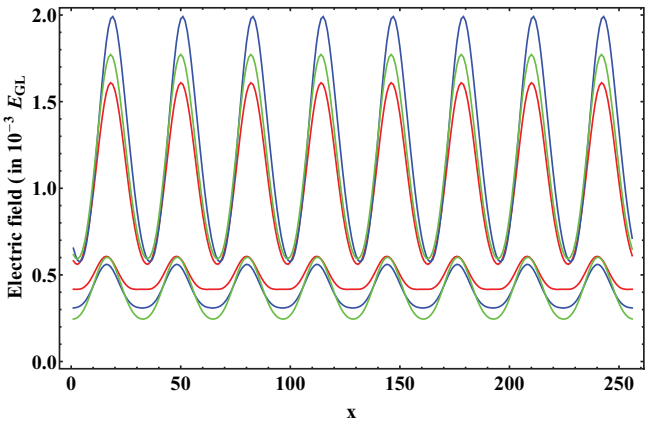


FIG. 7. (Color) Local electric-field distribution for $f = 4$. Profile of the electric field (in units of $E_{GL}$) for $y = L_y/2$ as function of $x$ for two values of the transport current. Slightly below the critical current $j_c = 0.003$ at $j = 0.002$ (three bottom lines for three consequent moments), there are just small fluctuations, and just above the critical current at $j = 0.004$, there are large variations with large amplitudes.

with the analytical estimate of electric field coherence length.[11] The *I-V* curve approaches the Bardeen-Stephen law, and the structure is very similar to that of the time-dependent GL model with renormalized viscosity,[19] namely, the friction owing to artificial pinning centers is accounted for by the increase of the effective inverse diffusion constant in the GL equation (17).

It is interesting to contrast our simulation in the channel geometry with that of the vortex transport in narrow channels.[20] In the latter case vortices are considered as a one-dimensional Frenkel-Kontorova chain.[21] In this model the potential is periodic [$\cos(x)$], with the period commensurate with the vortex lattice forming the channel. In this case vortex chains inside the channel create one-dimensional spatial structures (solitons). In our simulations, even for the relatively small width of the sample (of order of 5 pins in the $y$ direction), an essentially 2D structure, the snakes, are fully formed.

It is interesting to compare between the periodic pinning and the random pinning (always present in superconductors owing to disorder on a microscopic scale). Experiments were made in which a fraction of pins was distributed at random.[10] Within the London approximation such a system was studied very recently.[22] It would be interesting to investigate this phenomenon within the GL approach because the experiments fall clearly into its applicability range.

Very recently measurements were performed on a sample with a square pinning array,[23] which demonstrated jumps and a rather chaotic behavior and a transition between the snakes and a streamlike straight trajectories. It is difficult to compare with our results at small velocities because repulsive interaction favors a hexagonal vortex lattice that is constantly frustrated by the incommensurate square lattice of the pinning arrays. Nevertheless, we also observe jumps and turbulent behavior of the electric field accompanying vortex dynamics at the crossover between the snakelike and the straight trajectories. This requires additional analysis, which will be reported elsewhere.

## ACKNOWLEDGMENTS

We appreciate useful discussions with V. Vinokur, A. Gurevich, and B. Y. Zhu, and acknowledge support from the Israel Scientific Foundation (Grant No. 4/03-11.7). The work of B.R. was supported by NSC of R.O.C. under Grant No. 8907384-98N097 and MOE ATU program. B.R. acknowledges the hospitality and support of the Physics Department of Bar Ilan University.



[1] A. T. Fiory, A. F. Hebard, and S. Somekh, Appl. Phys. Lett. **32**, 73 (1978); M. Montero, O. Stoll, and I. Schuller, Europhys. J. B **40**, 459 (2004); U. Welp, X. L. Xiao, V. Novosad, and V. K. Vlasko-Vlasov, Phys. Rev. B **71**, 014505 (2005); A. A. Zhukov, E. T. Filby, P. A. J. de Groot, V. V. Metlushko, and B. Ilic, Physica C **404**, 166 (2004).

[2] J. I. Martín, M. Vélez, J. Nogués, and I. K. Schuller, Phys. Rev. Lett. **79**, 1929 (1997); D. J. Morgan and J. B. Ketterson, *ibid.* **80**, 3614 (1998); M. J. VanBael, K. Temst, V. V. Moshchalkov, and Y. Bruynseraede, Phys. Rev. B **59**, 14674 (1999); J. E. Villegas, E. M. Gonzalez, Z. Sefrioui, J. Santamaria, and J. L. Vicent, *ibid.* **72**, 174512 (2005); Q. H. Chen, G. Teniers, B. B. Jin, and V. V. Moshchalkov, *ibid.* **73**, 014506 (2006); J. E. Villegas, M. I. Montero, C.-P. Li, and I. K. Schuller, Phys. Rev. Lett. **97**, 027002 (2006).

[3] A. Yu. Aladyshkin1, A. V. Silhanek, W. Gillijns, and V. V. Moshchalkov, Supercond. Sci. Technol. **22**, 053001 (2009).

[4] H. J. Jensen, A. Brass, Y. Brechet, and A. J. Berlinsky, Phys. Rev. B **38**, 9235 (1988); A. C. Shi and A. J. Berlinsky, Phys. Rev. Lett. **67**, 1926 (1991); B. Y. Zhu, J. Dong, and D. Y. Xing, Phys. Rev. B **57**, 5063 (1998); H. Fangohr, S. J. Cox, and P. A. J. de Groot, *ibid.* **64**, 064505 (2001); A. B. Kolton, D. Dominguez, and N. Gronbech-Jensen, Phys. Rev. Lett. **86**, 4112 (2001).

[5] C. Reichhardt, C. J. Olson, and F. Nori, Phys. Rev. Lett. **78**, 2648 (1997); Phys. Rev. B **58**, 6534 (1998); C. Reichhardt, G. T. Zimanyi, and N. Gronbech-Jensen, *ibid.* **64**, 014501 (2001); C. Reichhardt and C. J. Olson Reichhardt, e-print arXiv:0808.1579v1.

[6] C. Reichhardt and C. J. Olson Reichhardt, Phys. Rev. B **79**, 134501 (2009).

[7] J.-Y. Lin, M. Gurvitch, S. K. Tolpygo, A. Bourdillon, S. Y. Hou, and J. M. Phillips, Phys. Rev. B **54**, R12717 (1996); S. Goldberg, Y. Segev, Y. Myasoedov, I. Gutman, N. Avraham, M. Rappaport, E. Zeldov, T. Tamegai, C. W. Hicks, and K. A. Moler, *ibid.* **79**, 064523 (2009).

[8] M. Kemmler, D. Bothner, K. Ilin, M. Siegel, R. Kleiner, and D. Koelle, Phys. Rev. B **79**, 184509 (2009).

[9] B. Rosenstein, I. Shapiro and B. Ya. Shapiro, Phys. Rev. B **81**, 064507 (2010).

[10] T. Hwa, D. R. Nelson, and V. M. Vinokur, Phys. Rev. B **48**, 1167 (1993).

[11] N. Kopnin, *Vortices in Type II Superconductors: Structure and Dynamics* (Landau Institute for Theoretical Physics, Moskow, 1995).

[12] I. Aranson, B.Ya. Shapiro, and V. Vinokur, Phys. Rev. Lett. **76**, 142 (1996).

[13] G. R. Berdiyorov, A. K. Elmurodov, F. M. Peeters, and D. Y. Vodolazov, Phys. Rev. B **79**, 174506 (2009).

[14] M. V. Miloŝevic and F. M. Peeters, Phys. Rev. Lett. **93**, 267006 (2004); G. R. Berdiyorov, M. V. Miloŝevic, and F. M. Peeters, Europhys. Lett. **74**, 493 (2006); Phys. Rev. B **74**, 174512 (2006).

[15] T. Maniv, B. Rosenstein, I. Shapiro, and B. Ya. Shapiro, Phys. Rev. B **80**, 134512 (2009).

[16] M. Ghinovker, I. Shapiro, and B. Ya. Shapiro, Phys. Rev. B **59**, 9514 (1999).

[17] J. Blatter, M. V. Feigelman, V. B. Geshkenbein, A. I. Larkin, and V. M. Vinokur, Rev. Mod. Phys. **66**, 1125 (1994); B. D. Tinh, D. Li, and B. Rosenstein, Phys. Rev. B **81**, 224521 (2010).

[18] H. J. Rothe, *Lattice Gauge Theories* (World Scientific, London, 2005).

[19] D. Li, A. M. Malkin, and B. Rosenstein, Phys. Rev. B **70**, 214529 (2004).

[20] A. Pruymboom, P. H. Kes, E. van der Drift, and S. Radelaar, Phys. Rev. Lett. **60**, 1430 (1988); N. Kokubo, R. Besseling, V. M. Vinokur, and P. H. Kes, *ibid.* **88**, 247004 (2002); R. Besseling, R. Niggebrugge, and P. H. Kes, *ibid.* **82**, 3144 (1999); R. Besseling, T. Dröse, V. M. Vinokur, and P. H. Kes, Europhys. Lett. **62**, 419 (2003).

[21] O. M. Braun and Yu. S. Kivshar, Phys. Rep. **306**, 1 (1998); T. Strunz and F. J. Elmer, Phys. Rev. E **58**, 1601 (1998); A. Vanossi, G. Santoro, V. Bartolani, J. Phys. Condens. Matter **16**, S2895 (2004).

[22] W. V. Pogosov, V. R. Misko, H. J. Zhao, and F. M. Peeters, Phys. Rev. B **79**, 014504 (2009).

[23] J. Gutierrez, A. V. Silhanek, J. Van de Vondel, W. Gillijns, and V. V. Moshchalkov, Phys. Rev. B **80**, 140514(R) (2009).